The modulation of stationary waves, and their response to climate change, by parameterized orographic drag

The Modulation of Stationary Waves, and Their Response to Climate Change, by Parameterized Orographic Drag

ANNELIZE VAN NIEKERK

Department of Meteorology, University of Reading, Reading, Berkshire, United Kingdom

JOHN F. SCINOCCA

Canadian Centre for Climate Modelling and Analysis, Victoria, British Columbia, Canada

THEODORE G. SHEPHERD

Department of Meteorology, University of Reading, Reading, Berkshire, United Kingdom

(Manuscript received 15 March 2017, in final form 19 May 2017)

ABSTRACT

The parameterization of orographic drag processes in atmospheric models remains uncertain because of a lack of observational and theoretical constraints on their formulation and free parameters. While previous studies have demonstrated that parameterized orographic drag acting near the surface has a significant impact on the atmospheric circulation, this work follows a more systematic approach to investigate its impacts on the large-scale circulation and the circulation response to climate change. A set of experiments with a comprehensive atmospheric general circulation model is used to ascertain the range of climatological circulations that may arise from parameter uncertainty. It is found that the Northern Hemisphere (NH) wintertime stationary wave field is strongly damped over the North Pacific (NP) and amplified over the North Atlantic (NA) as a result of increased low-level parameterized orographic drag, both of which are shown to be conducive to higher-latitude westerlies. A comparison with the stationary wave field presented in other studies suggests that the too-zonal NA jet and equatorward NP jet biases that are prevalent in climate models may be at least partly due to their representation of orographic drag. The amplitude of the stationary wave response to climate change across the experiments is shown to scale with the magnitude of low-level parameterized orographic drag through its influence on the present-day climatological stationary wave amplitudes over different sectors of the NH, which is consistent with linear stationary wave theory. This work highlights the importance of fidelity in a model's basic state for regional climate change projections.

1. Introduction

Climate models are heavily reliant on the parameterization of subgrid-scale physical processes within the atmosphere and ocean. In contrast to convection, which is generally entirely parameterized within climate models, orographic drag processes are partly resolved by the dynamics of the model and partly parameterized. In addition to the lack of observational constraints on orographic drag processes, the exchange between resolved and parameterized orographic drag as resolution is varied adds another level of uncertainty to the formulation of orographic drag parameterization schemes. van Niekerk et al. (2016) showed that, in the Met Office Unified Model (MetUM) at climate model resolutions, the decrease in parameterized orographic drag that occurs with increasing horizontal resolution was not balanced by an increase in resolved orographic drag. The inability of the model to maintain an equivalent total (resolved plus parameterized) orographic drag across resolutions resulted in an increase in systematic model biases at lower resolutions identifiable over short time scales.

As well as the impact that parameterized orographic drag from vertically propagating gravity waves has on the circulation (Palmer et al. 1986; McFarlane 1987), the impact of parameterizing the orographic drag that acts near the surface of the atmosphere (low-level parameterized orographic drag) has been shown to be beneficial

Corresponding author: Annelize van Niekerk, annelize.vanniekerk@metoffice.gov.uk

DOI: 10.1175/JAS-D-17-0085.1

for numerical weather prediction scores (Lott and Miller 1997), although it remains highly uncertain between models (Zadra et al. 2013). Sandu et al. (2016) demonstrated that, even if a model retains its total low-level parameterized orographic drag, a change in the relative contributions from two different parameterized orographic drag processes can lead to large quantitative differences in the model's circulation and forecast scores. However, less is known about the circulation sensitivity to low-level parameterized orographic drag processes in climate models, a topic which has only recently become of interest. Pithan et al. (2016) showed that the removal of low-level parameterized orographic drag in the MetUM can lead to a change in the circulation that is reminiscent of phase 5 of the Coupled Model Intercomparison Project (CMIP5) multimodel mean biases. Specifically, these biases include a too-zonal Northern Hemisphere (NH) circulation and a lack of tilt in the North Atlantic (NA) jet. The tilt in the NA jet has for a long time been associated with not only large-scale orographic features (Charney and Eliassen 1949; Grose and Hoskins 1979; Brayshaw et al. 2009; and several others) but also orographic forcing at small scales (Tibaldi 1986). The recent literature on the role of parameterized orographic drag for model circulation, although growing, is sparse and in need of a more systematic investigation, as is offered in the first part of this paper.

The CMIP5 ensemble has revealed that the systematic biases among models are often considerably larger than the response to climate change (e.g., Zappa et al. 2013). While it is well known that the wide range of sea surface temperatures (SST) and sea ice changes seen across climate models play a major role in the spread seen in the circulation response to climate change (Manzini et al. 2014), the role of the climatological basic state, and biases therein, is less clear. Previous studies, several of which were focused on the Southern Hemisphere (SH) circulation (Kidston and Gerber 2010; Barnes and Hartmann 2010; Simpson and Polvani 2016), have shown that there are relationships between the climatological basic state and the response to climate change (Sigmond and Scinocca 2010; Shepherd 2014, and references therein). The importance of model fidelity for predictive skill on seasonal time scales has also been recognized (Kharin and Scinocca 2012; Delsole and Shukla 2010). It is therefore a worthwhile exercise to investigate the sensitivity of the circulation response to climate change to a reduction in model bias in a controlled way, such as changes in the climatological basic state brought about by changes in orographic drag parameterization. This study aims to address this issue by first investigating the impact that varying orographic drag parameters has on the circulation within a comprehensive global circulation model and then asking the question: Does the circulation sensitivity to parameterized orographic drag matter for the climate change response?

The structure of the paper is as follows. In section 2 we describe the experimental design, model setup, experiments performed, and the details of diagnostics used in our analysis. In section 3 the response of the climatological zonal and meridional winds to systematic variations in the magnitude of parameterized drag is investigated. The responses of these two wind components are tied together by looking at the relationship between the latitudinal position of the zonal winds and the stationary wave amplitudes in both reanalysis and our experiments. The implications of this for the response to climate change in our experiments are described in section 4. Finally, the conclusions are synthesized and implications are discussed in section 5.

2. Experimental setup

To examine the influence that the uncertainty in low-level parameterized orographic drag may have on the climatological circulation and its response to climate change, we perform controlled experiments with a single model, the Fourth Generation Canadian Atmospheric General Circulation Model (CanAM4.1). CanAM4.1 has a spectral dynamical core and uses a hybrid vertical pressure coordinate system (Laprise and Girard 1990). Providing the atmospheric component to the Canadian Earth System Model (CanESM), it makes up part of the CMIP5 ensemble. The configuration employed in this study is that of a triangular truncation at T63, resulting in a (Gaussian) gridpoint resolution of 192×96 with a physics grid at a resolution of 128×64 grid points in the longitudinal and latitudinal directions, respectively, and 49 levels in the vertical extending to 1 hPa. Full details of the model dynamics and physics can be found in Scinocca et al. (2008) and von Salzen et al. (2013).

Repeated annual-cycle boundary conditions of SSTs and sea ice are prescribed so as to remove atmosphere–ocean and sea ice feedbacks as well as the additional interannual variability of the climate system that arises from these. In what we refer to as the $1\times CO2$ experiments, the atmospheric concentration of CO_2 is fixed at preindustrial levels, and sea ice and SST fields are generated using 100 yr of data from a preindustrial ocean–atmosphere coupled simulation performed with CanESM4.1 using the operational settings of the orographic drag parameterization scheme (i.e., experiment

TABLE 1. Description of perturbed parameterized orographic drag experiments. Columns are, from left to right, name of experiment; value of 2D and 3D blocking coefficients; whether or not experiment has downslope wind drag turned on; and length of experiment at both 1×CO2 and 2×CO2.

Expt	Blocking coefficient CD = (2D, 3D)	Downslope wind?	Length (yr)
[0, 0]	CD = (0, 0)	No	60
[*B*, 0]	CD = (1.0, 0.5)	No	60
[0, *D*]	CD = (0, 0)	Yes	80
[*B*, *D*]	CD = (1.0, 0.5)	Yes	80
[*B* + , 0]	CD = (7.0, 2.0)	No	60
[*B* + , *D*]	CD = (7.0, 2.0)	Yes	80

[B, D] in Table 1). In the climate change experiments, referred to as the 2×CO2 experiments, CO_2 is doubled, and SSTs and sea ice are also derived from coupled simulations, in which CO_2 is doubled relative to preindustrial levels. The doubled-CO_2 coupled simulations are run for 140 yr, and a climatological annual cycle of SSTs and sea ice is derived from the final 30 yr, at which point global-mean SSTs have reached approximate equilibrium.

The global-mean annual-mean surface temperature perturbation is ~3.5 K in these experiments, placing it near the 8.5 representative concentration pathway (RCP8.5) response in the CMIP5 multimodel mean at the end of the twenty-first century (Golledge et al. 2015). Both the response to climate change and the response to perturbations in the parameterized drag are largest during NH winter, which is why this study is focused on the mean over December–February (DJF) and all analysis is performed over this period.

a. Orographic drag parameterization

CanAM4.1 employs the orographic drag parameterization scheme described by Scinocca and McFarlane (2000, hereafter SM00), which accounts for unresolved orography through three processes: vertical fluxes of momentum from topographically forced freely propagating gravity waves; drag enhancement as a result of low-level wave breaking (i.e., downslope windstorm behavior); and, finally, low-level flow blocking. Transitions between these processes are discerned through the inverse Froude number, a nondimensional measure of the nonlinearity of the topographic forcing, given by $\mathrm{Fr} = Nh/U$, where h is the subgrid mountain height and N and U are bulk measures of the buoyancy frequency and wind speed upstream of the subgrid topography, respectively. It should be noted that, while the treatments of each of these three processes are distinct, there is considerable overlap of the Fr values over which they are operable (SM00). Idealized modeling studies and observational campaigns have provided an approximate characterization of the response to orographic forcing under different Fr regimes. In regions where the flow is blocked ($\mathrm{Fr} \geq \mathrm{Fr}_{\mathrm{crit}}$, with $\mathrm{Fr}_{\mathrm{crit}} = 1$) the drag over the height of the blocked layer is parameterized in the following form:

$$D(z) \propto -\frac{\sigma_x}{\sigma}\rho_0 C_d U|U|,$$

where σ_x is the slope of the subgrid orography, σ is the standard deviation of the subgrid orography, ρ_0 is the low-level density, C_d is the drag coefficient, and U is the low-level wind. The drag coefficient C_d is a free parameter and takes on different values for the two-dimensional and three-dimensional properties of the subgrid orography (see SM00 for exact formulation).

In this study, we focus primarily on the impact of low-level flow blocking on the circulation response by systematically varying the C_d parameter within the blocking component of the orographic drag scheme. The C_d values used in our experiments are within the range of what is found from laboratory experiments (Vosper 2000) and is used in other models. The sensitivity of its impact to the presence of low-level wave breaking is evaluated by switching the downslope drag enhancement on and off in the SM00 scheme. This leads to the set of six model configurations listed in Table 1, which were executed at both 1×CO2 and 2×CO2. Taken together, the set of six SM00 configurations may additionally be viewed as systematically increasing the total low-level drag, and they have been ordered in Table 1 to reflect increasing drag moving down the table. While systematic, this increase in drag is not completely linear over all regions because of compensation by other surface drag processes, such as the boundary layer drag and the Froude number dependence of the parameterized components. For reference, the configuration labeled [B, D] in Table 1 is the default setting of the SM00 scheme in CanESM4.1.

Delineating the sensitivity of the atmospheric circulation to the different configurations in Table 1 can be difficult because of internal variability of the climate system. This is particularly the case for processes that have an impact over regions with large variability, such as the impact that parameterized orographic drag has on storm tracks (Pithan et al. 2016). This motivated the use of cyclostationary 1×CO2 preindustrial and 2×CO2 perturbed AGCM-only simulations that could be executed for a period of time deemed necessary to separate such circulation sensitivities from the internal variability of the climate system. The lengths of integrations employed for each configuration in this study are also listed in Table 1.

b. Momentum budget calculation

The zonal-mean vertically integrated momentum budget of the atmosphere on pressure levels is given by

$$\frac{\partial}{\partial t}\langle[u]\rangle = -\frac{1}{a\cos^2\phi}\frac{\partial}{\partial\phi}\langle[uv]\rangle\cos^2\phi - \left[\frac{p_s}{a\cos\phi}\frac{\partial h_s}{\partial\lambda}\right] + \langle[fv]\rangle + \langle[F_\lambda]\rangle, \quad (1)$$

where u and v are the zonal and meridional winds, respectively, a is the radius of Earth, ϕ is latitude, p_s is the surface pressure, h_s is the surface elevation, λ is longitude, f is the Coriolis parameter, and F_λ is the tendency from parameterized processes. In (1), $[(\cdots)]$ indicates a zonal mean, and $\langle(\cdots)\rangle = \int_{p_{\text{top}}}^{p_s}(\cdots)\,dp/g$ is the vertical integral from the surface to the model top. In CanAM4.1 F_λ has contributions from boundary layer turbulent mixing and parameterized orographic drag as well as negligible contributions from convective entrainment of momentum and horizontal diffusion. Momentum budget terms are calculated from 6-hourly output on model levels, and spatial derivatives are calculated in spectral space so as to be consistent with model numerics.

The time-mean momentum flux convergence (MFC), the first term on the right-hand side of (1), can be broken down into transient and stationary components:

$$-\frac{1}{a\cos^2\phi}\frac{\partial}{\partial\phi}\langle[\overline{u}\,\overline{v}]\rangle\cos^2\phi = -\frac{1}{a\cos^2\phi}\frac{\partial}{\partial\phi}\langle[\overline{u'v'}]\rangle\cos^2\phi - \frac{1}{a\cos^2\phi}\frac{\partial}{\partial\phi}\langle[\overline{u}\,\overline{v}]\rangle\cos^2\phi, \quad (2)$$

where overbars indicate a time mean and primes indicate a departure from the time mean. The stationary component can be further broken down into its zonal and eddy components such that

$$-\frac{1}{a\cos^2\phi}\frac{\partial}{\partial\phi}\langle[\overline{u}\,\overline{v}]\rangle\cos^2\phi = -\frac{1}{a\cos^2\phi}\frac{\partial}{\partial\phi}\langle[\overline{u}^*\overline{v}^*]\rangle\cos^2\phi - \frac{1}{a\cos^2\phi}\frac{\partial}{\partial\phi}\langle[\overline{u}][\overline{v}]\rangle\cos^2\phi, \quad (3)$$

where an asterisk denotes a deviation from the zonal mean. The first term on the right-hand side of (3) is the stationary eddy momentum flux convergence (SEMFC), and the second term is the stationary zonal-mean momentum flux convergence. While we do not calculate the contribution from the transient component explicitly, the stationary component is derived from climatological DJF-mean values of u and v on pressure levels.

The motivation for looking at the momentum budget comes from the fact that the interaction between the surface drag and the momentum fluxes is two way, such that, in the steady state limit, the predominant balance is between the momentum flux convergence and the surface drag. Understanding the extent to which low-level orographic drag plays a role in the structure of the circulation is, therefore, best aided by looking at how the momentum fluxes, and their stationary and transient contributions, are balanced or affected by surface drag.

c. Jet latitude calculation

The jet latitude is calculated using

$$\phi_{\max} = \frac{\sum_{\phi([u]\geq 0)}^{\phi_{\text{pole}}}[u(\phi)]^2\phi}{\sum_{\phi([u]\geq 0)}^{\phi_{\text{pole}}}[u(\phi)]^2}, \quad (4)$$

where $[u]$ is the zonal wind averaged over some sector, $\phi([u]\geq 0)$ is the latitude at which the zonal winds over that sector become positive, and ϕ_{pole} is the most poleward latitude considered, set as 75°N over the NH and 75°S over the SH.

Relative to the usual latitude of the jet maximum that is often quoted in the literature, $\phi_{\max}$ provides a bulk measure of the structure of the jet and its response since it integrates over the entire jet region and so is able to account for features such as a bimodal distribution or a tilt in the jet, as is found over the North Atlantic (Woollings et al. 2010). The sectors discussed in what follows are defined as the average zonal winds over the following: the NH 15°–75°N, 0°–360°E; NA sector 15°–75°N, 30°W–30°E; North Pacific (NP) sector 15°–75°N, 150°–240°E; and SH 15°–75°S, 0°–360°E. The NP and NA sectors are chosen to correspond with the regions of the largest changes seen in response to increasing the parameterized orographic drag. The climatological jet latitude is then calculated from the climatological DJF zonal winds at 850 hPa.

d. Regression analysis

It is understood from theoretical, observational, and modeling studies that the amplitude, phase, and location of low-frequency waves are strongly related to the modes of jet variability within the atmosphere (Rossby 1939; Wallace and Hsu 1985; Ting et al. 1996), with anomalous stationary wave momentum fluxes over the NA being associated with a more poleward-tilted NA jet, relative to its climatology (Limpasuvan and Hartmann 2000; DeWeaver and Nigam 2000). The internal variability of the atmosphere can therefore be exploited to understand the relationship between the stationary wave forcing on the mean flow, its location

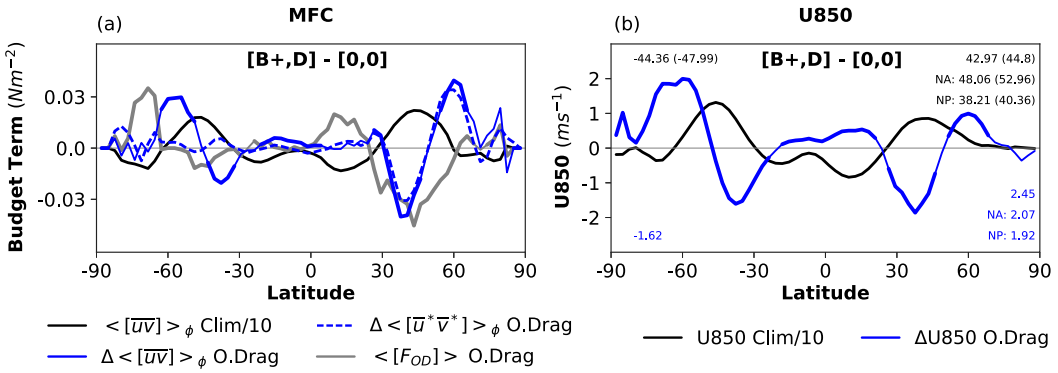

FIG. 1. (a) DJF 1×CO2 MFC climatology divided by 10 (solid black line) and response to parameterized orographic drag (solid blue line). The solid gray line is the zonal-mean total (freely propagating, blocking, and downslope wind) parameterized orographic stress F_{OD} at 1×CO2. The dashed blue line is the SEMFC response to drag. (b) DJF 1×CO2 u 850-hPa climatology divided by 10 (solid black line) and response to drag (solid blue line). See text for description of values quoted in (b). Regions of statistically significant differences (at the 95% level based on the two-sided independent Student's t test) are indicated by a thickening of the line.

and amplitude, and the jet latitude. We use regression analysis over different sectors of the NH to capture the spatial structure of the low-frequency wave forcing under different jet latitude regimes. To do this, we first generate a jet latitude index as a function of time by normalizing the monthly jet latitude anomalies by the maximum anomaly:

$$\alpha(m) = \frac{\phi_{\max}(m) - \overline{\phi}_{\max}}{\max(|\phi_{\max}(m) - \overline{\phi}_{\max}|)}, \tag{5}$$

where $\phi_{\max}(m)$ is calculated from the monthly mean zonal winds at 850 hPa using (4), and $\overline{\phi}_{\max}$ is the average of $\phi_{\max}(m)$ over all months considered. Thus, $\alpha(m)$ is generated for each December, January, and February between 1979 and 2016 from ERA-Interim monthly mean data.

Regressing the stationary Plumb flux vector $\mathbf{F}_p$, given by (5.7) in Plumb (1985), onto α gives

$$\mathbf{R} = \overline{\alpha(m)\mathbf{F}_p(m)}. \tag{6}$$

The values of α can be calculated for different sectors of the globe and gives an indication of the strength of the jet latitude anomaly. The time-mean covariance between α and $\mathbf{F}_p$, given by $\mathbf{R}$, can be seen as the difference between the stationary Plumb flux at anomalously high jet latitudes and anomalously low jet latitudes.

3. Response to orographic drag at 1×CO2

a. Zonal wind response to drag

We begin by looking at the circulation response to systematically increasing total parameterized orographic drag (i.e., from [0, 0] to [B+, D] in Table 1) at 1×CO2. The primary behavior of the response will be illustrated by focusing on the difference between experiments [B+, D] and [0, 0]. The spatial structure of the response to increased drag remains very similar across the configurations listed in Table 1, and, unless stated otherwise, the response amplitude increases as the low-level parameterized drag is increased (an example of the increasing amplitude of the response with increased drag is shown later in Fig. 6). This scaling of the response to drag, although not entirely linear, implies that the circulation response is robust and that configuration [B+, D] relative to [0, 0] is representative of this sensitivity. Figure 1a shows the 1×CO2 climatological MFC (divided by 10) for experiment [0, 0] in black and the total parameterized orographic drag (freely propagating wave drag, blocking drag, and downslope wind drag) acting on the zonal winds for experiment [B+, D] in gray. The change in the MFC in response to increasing the parameterized drag is plotted in solid blue. As is to be expected from the hemispheric distribution of land, the momentum flux response to increased orographic drag is larger in the NH than the SH. There is, however, large parameterized orographic drag located at 65°S, which is the latitude encompassing the Antarctic Peninsula. Large low-level drag over this region may be explained by the fact that the cold Antarctic region, with strong stratification, will have more flow trapped near the surface.

The climatological zonal-mean zonal wind at 850 hPa for [0, 0] is plotted in black in Fig. 1b, along with its response to increased drag in blue. The climatological surface winds and their response correspond well with the momentum fluxes and their response. There is an overall poleward migration of the circulation, as

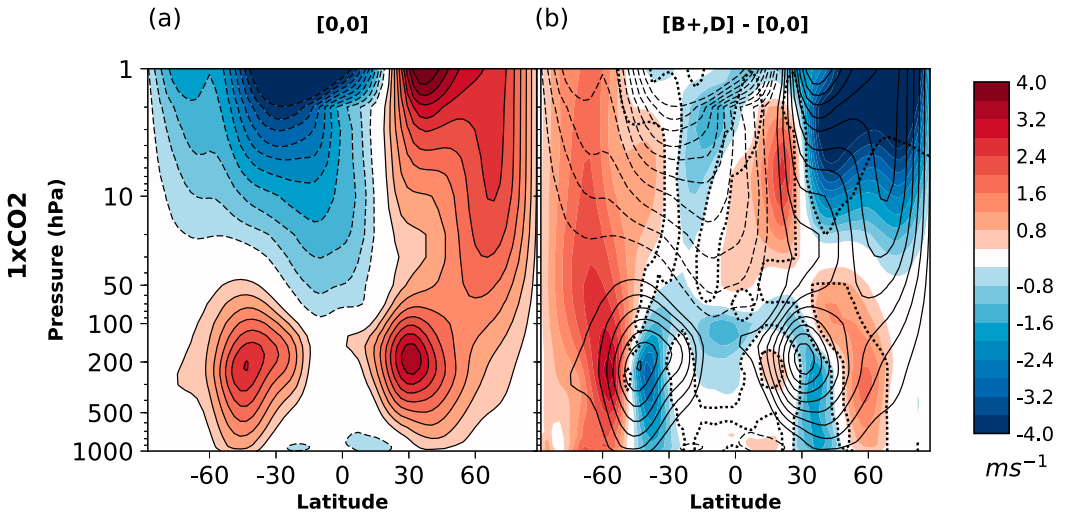

FIG. 2. DJF [u]. (a) The [0, 0] 1×CO2 climatology; contour interval is 5 m s^{-1}. (b) Line contours indicate [0, 0] climatology, and colored contours are the response to drag ([B+, D] minus [0, 0]), with contour interval given by the color bar. Regions of statistically significant differences (at the 95% level based on the two-sided independent Student's t test) are encompassed by dotted black lines, as is also the case in subsequent figures.

indicated by the jet latitude change quoted in blue. The values quoted in black are the climatological values in [0, 0], and the values in brackets are the jet latitudes calculated from ERA-Interim (Dee et al. 2011) using the DJF climatology from December 1979 to January 2016. From these jet latitude values, it can be concluded that the [0, 0] experiment has jets placed preferentially toward the equator in all sectors considered, relative to ERA-Interim. Across the experiments, the additional orographic drag shifts the jet toward the pole in all sectors with the magnitude of the shift increasing with increasing low-level drag. This acts to mitigate the jet biases, roughly cutting it in half in the SH and NA, and essentially eliminating it in the NH and NP. For comparison, Bracegirdle et al. (2013) showed that the SH zonal-mean jet latitude bias could be reduced by 28% when observed SSTs and sea ice are prescribed in place of coupling between the ocean/ice and atmosphere models. Here, the SH zonal-mean jet latitude bias is reduced by 44% when the low-level parameterized orographic drag is included, further demonstrating the large role of atmospheric processes in the SH jet latitude bias.

Although the deceleration felt by the atmosphere from the additional parameterized drag acts only near the surface, the response may not necessarily be confined to the lower part of the atmosphere. A similar poleward migration of the circulation within the troposphere can be seen in Fig. 2, which shows the 1×CO2 climatological zonal-mean zonal winds for [0, 0] in Fig. 2a and their response to increased drag in Fig. 2b as a function of pressure. The response to the increased drag is vertically coherent within the midlatitude troposphere. The date of the transition to easterlies in the SH stratosphere has been shown to be hastened by an increase in the freely propagating wave component of the parameterized orographic drag (McLandress et al. 2012), the magnitude of which is reduced as the low-level drag is increased (not shown). This may explain why, in the SH, the response extends far up through the atmosphere and appears as a deceleration of the easterlies in the SH polar stratosphere.

In contrast to the SH, the NH polar stratospheric winds decelerate with increasing low-level blocking drag, with only [B, D] exhibiting an acceleration of the polar stratosphere (not shown). There is, however, a lack of statistical significance over this region in [B, D], which suggests that this may be because of the large variability that is seen in the stratosphere during the NH winter season as a result of sudden stratospheric warmings. The deceleration of the stratospheric winds in response to increased low-level drag is similar to that found by Sandu et al. (2016), in experiments where the parameterized low-level orographic blocking was increased. This, as well as the four experiments that show a deceleration within the stratosphere, supports the idea that there is an increase in the wave forcing reaching the NH polar stratosphere when low-level drag is increased.

The longitudinal structure of the 850-hPa zonal wind response to drag is shown in Fig. 3 with, as before, the climatological values in [0, 0] in Fig. 3a and the response to increased drag in Fig. 3b. The largest changes occur at the jet exit regions over the NA and NP. As a point of reference, the ERA-Interim DJF climatological

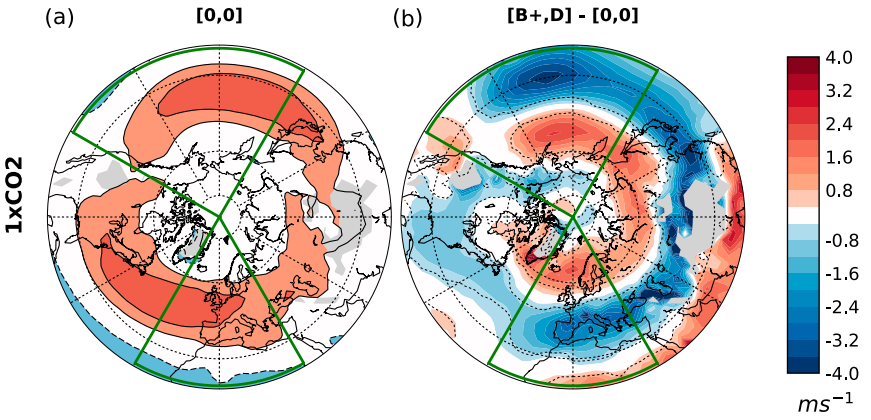

FIG. 3. DJF u 850 hPa. (a) 1×CO2 climatology in [0, 0]; contour interval is 5 m s^{-1}. (b) Response to drag, with contour interval given by the color bar.

850-hPa zonal winds are plotted in Fig. 4a. There are clear differences that can be seen by eye between the ERA-Interim climatology and the [0, 0] climatology: in the latter the NP jet is too strong at the jet exit and entrance regions, and the NA jet is too strong and zonal over western Europe. This is evidenced by the difference plotted in Fig. 4b. It is striking that the differences between the [0, 0] and ERA-Interim zonal winds match the structure of the response to increased drag, but with an opposite sign. It is, therefore, not surprising that the differences are much smaller between ERA-Interim and [B+, D], the experiment with the largest amount of low-level drag (Fig. 4c). This shows that, for the diagnostics considered here, the additional low-level drag is beneficial for the model fidelity of CanAM4.1.

It is clear from what has been discussed that the additional orographic drag has a nonnegligible impact on the zonal winds. To ascertain the mechanisms behind this sensitivity, we appeal again to the momentum budget calculations. As is found in both observations and models (Limpasuvan and Hartmann 2000; Simpson et al. 2014), the stationary eddies make a dominant contribution to the climatological momentum transport in the NH, whereas the transients account almost entirely for the momentum transport in the SH. A comparison of the total MFC and SEMFC response to increased drag, plotted in a dashed blue line in Fig. 1a, shows that the change in the zonal-mean zonal wind over the NH is also predominantly as a result of a change in the transport of momentum by the stationary eddies. In contrast, the zonal-mean zonal wind change in the SH is sustained by a change in the transient momentum flux convergence. While we recognize that the SH response to increased drag is important, the mechanisms are apparently more complex and not immediately apparent from our present analysis. Analysis of the SH response will, therefore, be left for future investigation. That said, the SH response is similar to the response to orographic blocking found by Pithan et al. (2016) using the MetUM and is consistent with the mechanism proposed in Chen

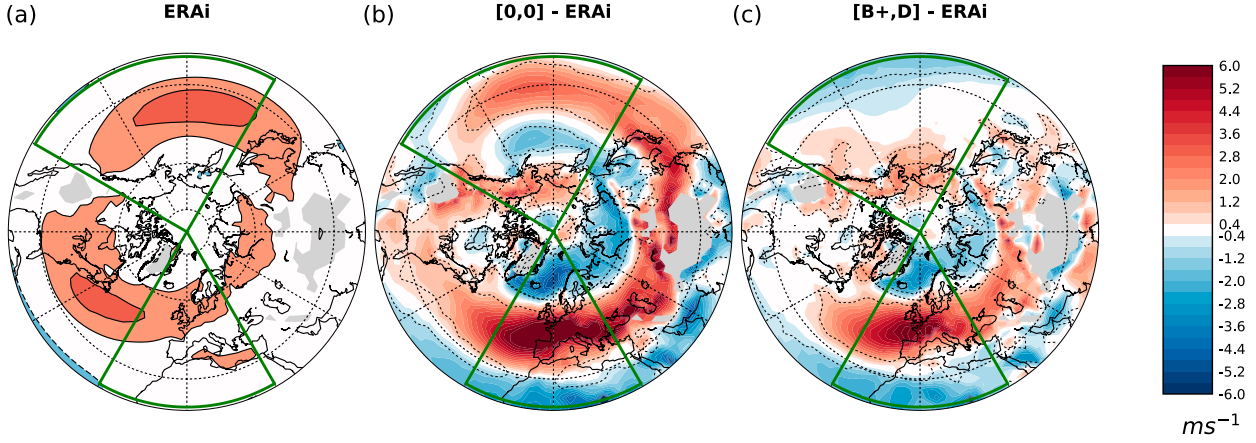

FIG. 4. DJF u 850 hPa. (a) ERA-Interim climatology, contour interval is 5 m s^{-1}. (b) [0, 0] minus ERA-Interim. (c) [B+, D] minus ERA-Interim. Contour interval in difference plots given by the color bar.

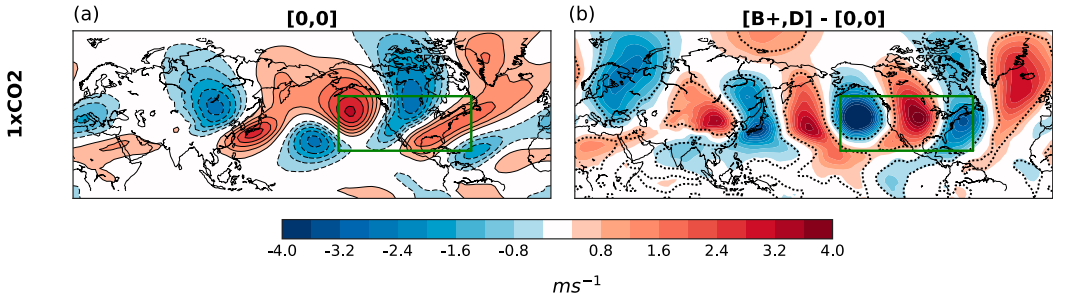

FIG. 5. DJF v^* 300 hPa. (a) [0, 0] 1×CO2 climatology; contour interval is 2 m s^{-1}. (b) Response to drag, with contour interval given by the color bar. Green boxes indicate the region used in calculating the RMS v^* amplitudes in Fig. 14.

and Zurita-Gotor (2008). They find that prescribing a positive zonal torque at the surface on the poleward flank of the jet maximum leads to a poleward shift of the midlatitude jet. The opposite is found for a torque placed on the equatorward flank of the jet maximum. In our experiments the additional orographic drag leads to both a positive torque on the poleward flank and a negative torque on the equatorward flank of the SH jet, which would be expected to result in a poleward shift by the arguments of Chen and Zurita-Gotor (2008).

b. *Stationary wave response to drag*

Since we know that it is the transport of momentum by the stationary eddies that sustains the zonal wind response to increased orographic drag in the NH, it is of interest to consider how the stationary wave field itself changes with increased drag. The zonally asymmetric meridional winds v^* at 300 hPa are used to visualize the stationary wave field. Climatological v^* at 300 hPa is plotted in Fig. 5a for [0, 0] and the response to drag in Fig. 5b. From the climatology, there is evidence of a wave train emanating from the Himalayan topography that reaches the North American coast where the flow is altered by the presence of the Rockies, acting to elongate the waves and aiding the characteristic jet tilt that is seen over the North Atlantic. As the parameterized drag is increased, the wave train over the Pacific is strongly damped, whereas the stationary waves over the higher-latitude NA are amplified.

To visualize this, the zonal wavenumber spectrum of v^* at 300 hPa is plotted as a function of latitude for [0, 0] on the far left of Fig. 6, and the response to drag across the experiments is plotted to its right. As was indicated by Fig. 5, the waves in the midlatitudes (predominantly over the central Pacific), which peak at zonal wavenumber 5, are systematically damped by the additional drag. At the high latitudes, v^* at wavenumber 2 is amplified. The localized change in the stationary wave forcing is illustrated in Fig. 7, which shows the 1×CO2 [0, 0] climatology (Fig. 7a) and response to drag (Fig. 7b) of the 700-hPa vertical (colored contours) and 300-hPa horizontal (vectors) components of the stationary Plumb flux computed from (5.7) of Plumb (1985). The zonal mean of the Plumb flux is equivalent to the EP flux for stationary waves. In regions where the vertical component is large there is an acceleration of the surface westerlies, and, in regions where the vectors are diverging meridionally, there is an acceleration of the

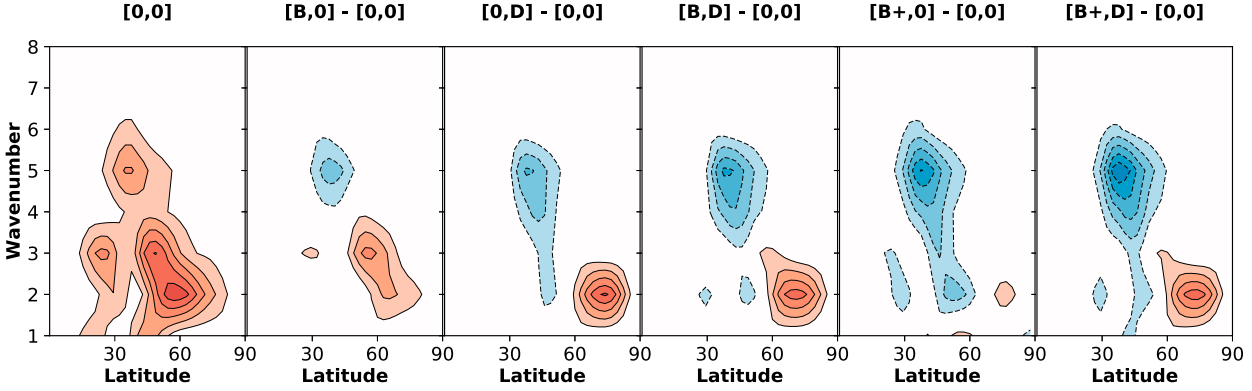

FIG. 6. DJF v^* 300-hPa zonal wavenumber vs latitude spectrum. (left) [0, 0] 1×CO2 climatology; contour interval is 5 m^2 s^{-2}. (right) Response to drag across the experiments (experiment minus [0, 0]). Contour interval is 2 m^2 s^{-2} in difference plots.

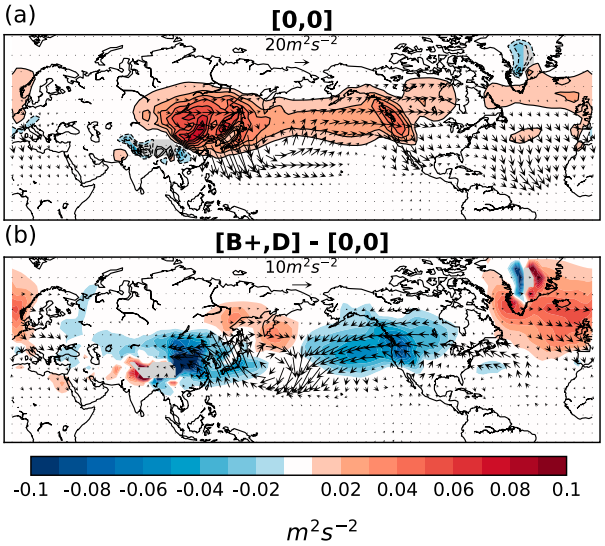

FIG. 7. DJF stationary Plumb flux. Colored contours are the vertical component at 700 hPa. Arrows are the horizontal component at 300 hPa, with their magnitude indicated by the key. (a) The [0, 0] 1×CO2 climatological Plumb flux; contour interval is $4\times10^{-2}\,\mathrm{m^2\,s^{-2}}$. (b) Response to orographic drag ([B+, D] minus [0, 0]), with contour interval given by the color bar.

westerlies at 300 hPa. As the low-level parameterized drag is increased, there is a large reduction in the vertical and meridional components downwind of the Himalayas and an increase over Siberia, which is consistent with a poleward movement of the NP zonal winds. Over the Rockies there is a decrease in the vertical component, which acts to reduce the surface westerlies. As is anticipated from the increased v^* amplitudes, there is an increase in the vertical and meridional components of the Plumb flux over the NA, which results in an increased forcing of the stationary waves and the zonal wind. This not only shows the longitudinal structure of the wave forcing but also demonstrates that the changes in the stationary waves are situated around the largest orography. This diagnostic aids the interpretation that damping of the waves in the midlatitudes over the NP, which leads to reduced zonal momentum and heat fluxes into that region by the stationary eddies, is a result of changes in the stationary waves originating from the topography, particularly the Himalayas.

The source of the stationary wave changes over the NA is less clear, and it is possible that the amplified stationary waves over the NA are a result of changes in the stationary waves originating from either the Rockies or Greenland (Junge et al. 2005). For the case in which changes in the stationary waves seen over the NA originate from the Rockies (although similar arguments may be applied to Greenland), there are two possible mechanisms for this response. In the first, the parameterized orographic drag acting over the Rockies directly alters the stationary wave generation over that region. In the second, the zonal wind changes that occur over the Pacific region, as a result of changes in the parameterized orographic drag over the Himalayas, alter the way in which the winds interact with the resolved Rocky Mountains, thus altering the downstream wave generation.

c. *Connection between jet latitude and stationary waves*

In section 2d, we described a regression analysis that utilizes the fact that the low-frequency variability of the NA and NP jet latitude is related to the momentum and heat fluxes by the stationary waves. This regression analysis is not capable of attributing cause and effect since it is only capturing the instantaneous covariance of the two fields. It is also possible that externally forced variations in jet latitude and stationary wave amplitude, such as those imposed by the stratosphere or diabatic heating, can have an impact on the relationship between these two fields. Nevertheless, if we wish to understand the contribution that the stationary waves make toward sustaining the jets at particular latitudes, we find this analysis a useful means to this end.

Figure 8 shows the normalized jet latitude anomalies for the NA and NP for the NH winter months (DJF) as a function of time calculated from ERA-Interim monthly mean zonal winds at 850 hPa. There is clearly a lot of interannual variability in jet latitude over the NA and NP, with the anomalies of the NA possibly appearing more persistent compared with those over the NP. Figure 9 shows the regression of α calculated over the NA and NP sectors, as shown in Fig. 8, on the stationary Plumb flux $\mathbf{F}_p$ given by (6). Looking first at the NA **R** field, the Plumb flux over the NA region that is associated with a more poleward NA jet tilt is that of increased vertical surface heat fluxes and upper-level meridional momentum fluxes over the NA. This is in contrast to the stationary wave field that is associated with a more poleward NP jet, which appears as a weakening of the vertical component of the Plumb flux over the west coast of North America and downwind of the Himalayas.

The analysis above suggests that a stronger climatological stationary wave pattern over the NA is associated with a more poleward-tilted NA jet and that a damping of the stationary waves over the NP is associated with a more poleward-positioned NP jet. Indeed, comparing Fig. 9 with the Plumb flux response to increased drag shown in Fig. 7, we see that the anomalous stationary wave fields that emerge from internal variability associated with more poleward jet latitudes are

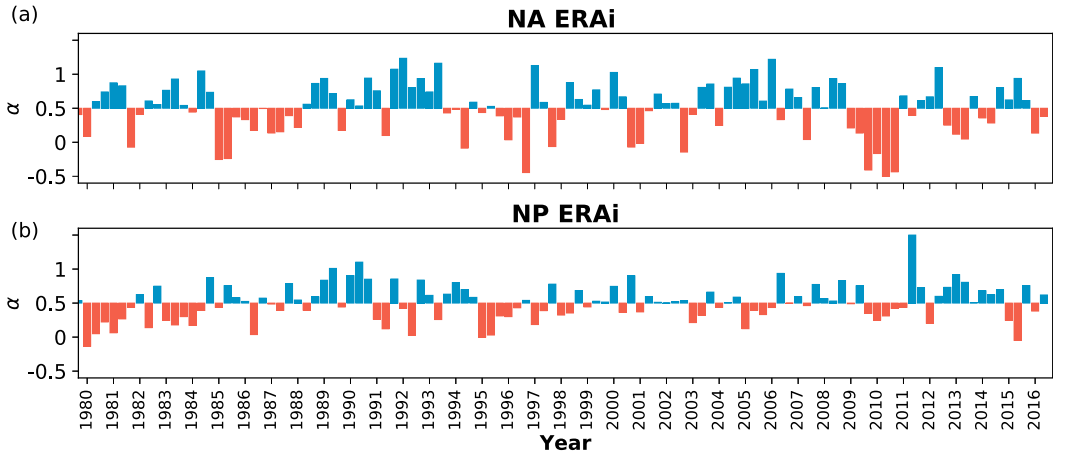

FIG. 8. Time series of α (see section 2d) calculated from monthly u 850-hPa values during the DJF season for ERA-Interim starting in December 1979 over (a) NA and (b) NP sectors given by green boxes in Fig. 3.

similar to the stationary wave response to increased orographic drag. From this, as well as findings by DeWeaver and Nigam (2000) and Ting et al. (1996), we may conclude that the stationary waves play an important role in sustaining regional jet latitude, and, on altering the climatological stationary waves, an associated change in the climatological jet latitudes is likely to be seen.

Figure 10 shows the relationship between the root-mean-square (RMS) v^* amplitude over the region 30°–90°N, 45°W–45°E and the jet latitude over the NA at 1×CO2 in the set of experiments and ERA-Interim. As is consistent with the regression analysis and the spectra shown in Fig. 6, the experiments with larger amounts of orographic drag, which tend to have larger stationary wave amplitudes over the NA, also tend to have a more poleward-tilted NA jet. What is more, the large stationary wave amplitudes in ERA-Interim also correspond well with a more poleward-tilted NA jet.

Figure 11 shows the climatological power spectrum of v^* as a function of wavenumber and latitude for ERA-Interim, [0, 0], and [B+, D]. The peak between 30°–40°N at wavenumber 5 in [0, 0] is not at all present in the reanalysis, and when the low-level drag is increased this peak is barely visible. The increase in wavenumber-2 amplitudes over the northern high latitudes also brings [B+, D] closer to the ERA-Interim climatology. Figure 4c of Simpson et al. (2016), which shows the CMIP5 multimodel mean climatological v^* spectrum, is similar to that of [0, 0] with weak wavenumber-2 amplitudes at high latitudes, relative to ERA-Interim, and a peak at wavenumber 5. The discussion above, along with the v^* spectrum presented in Simpson et al. (2016), suggests that the too-zonal NA jet and equatorward NP jet biases that are prevalent in climate models are connected with the too-weak stationary waves over the NA and too-strong stationary waves over the NP. A similar conclusion was drawn by Pithan et al. (2016), who found that increased parameterized orographic drag led to an improved representation of the North Atlantic jet tilt and, as a result, an improved storm-track density over that region.

4. Climate change response

We have shown that there are large changes in the climatological circulation, primarily in the stationary wave field, when the low-level parameterized orographic drag is systematically altered across our experiments (i.e., Table 1). Since the configurations described in Table 1 are forced with the same SSTs and sea ice, it is easier to disentangle the often alluded to but difficult to quantify connection between the climatological basic state of the model and its response to climate change. With this in mind, the following analysis addresses this issue in the context of climatological stationary waves and their response to climate change.

a. Stationary wave response to climate change

Simpson et al. (2016) showed that the amplitude of the stationary wave response over the southwest interior of North America in the CMIP5 ensemble was dependent not only on the historical stationary wave amplitudes but also on the zonal-mean zonal wind response to climate change. As a result, we begin the discussion by looking at the latter. Figure 12a shows the zonal-mean zonal wind response to climate change in [0, 0]. The difference between the response to climate change in [B+, D] and the response in [0, 0] is shown in colored contours in Fig. 12b, with the full response in [0, 0] repeated in line

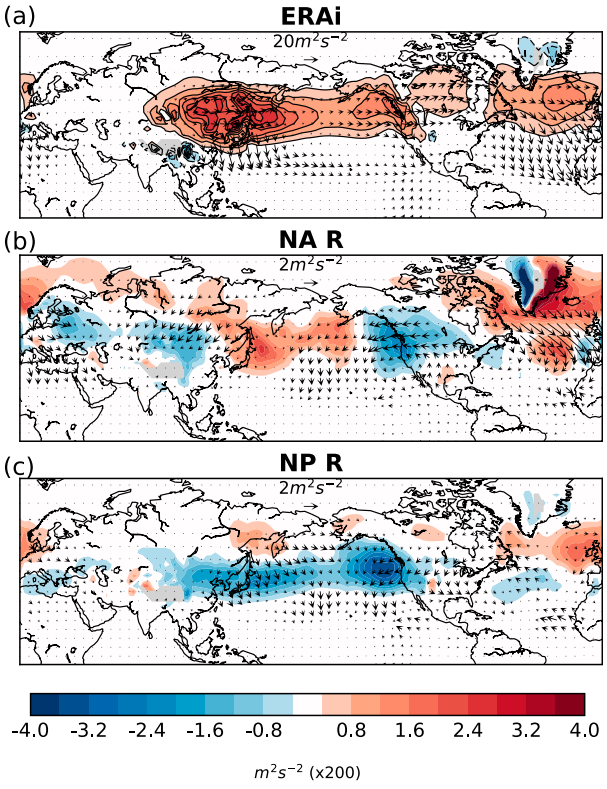

FIG. 9. (a) DJF stationary Plumb flux calculated for ERA-Interim. Colored contours are the vertical component at 700 hPa; contour interval is 4×10^{-2} m^2 s^{-2}, and arrows are the horizontal component at 300 hPa, with their magnitude indicated by the key. The time-mean covariance **R** [see (6)] for ERA-Interim over DJF season calculated for (b) the NA sector and (c) the NP sector. Colored contours are the vertical component at 700 hPa, with the contour interval given by the color bar (×200), and arrows are the horizontal component at 300 hPa, with their magnitude indicated by the key.

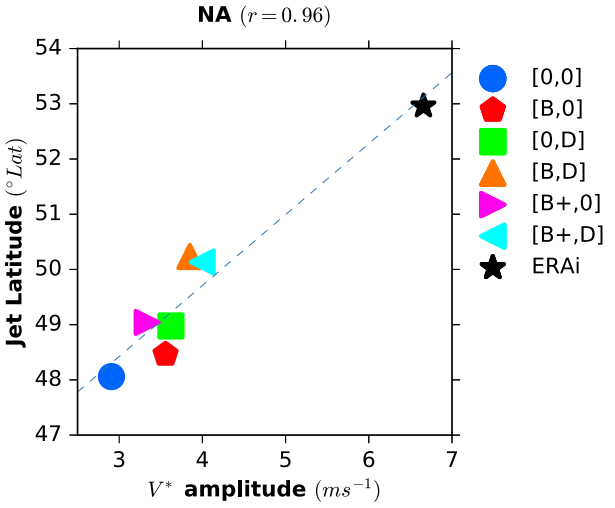

FIG. 10. Relationship between RMS v^* 300-hPa amplitude over the NA and the NA jet latitude for the drag experiments at 1×CO2 and ERA-Interim (ERAi).

contours. We note the typical features of the zonal wind response to climate change that are robust across models, such as the poleward movement of the SH jet and the strengthening of the winds in the subtropics that result from subtropical upper-tropospheric amplification of surface warming (e.g., Butler et al. 2010). There is, however, a lot of uncertainty in the Northern Hemisphere high-latitude tropospheric and stratospheric circulation response in climate models, which is often linked to the interplay between the strength of the Arctic and subtropical upper-tropospheric amplification (Manzini et al. 2014). Although the CMIP5 multimodel mean NH midlatitude jet response is a poleward shift in DJF (Barnes and Polvani 2013), there is a lot of spread about this mean, and the zonal wind response seen in these experiments is just one possible outcome under climate change. Relative to the CMIP5 ensemble, these experiments have an average amount of polar amplification, a deceleration of the stratospheric winds, and a weak subtropical amplification, which is consistent with less of a poleward shift of the NH zonal winds (Zappa and Shepherd 2017). What is clear from the difference in the climate change response (Fig. 12b) is that the additional low-level parameterized orographic drag has no significant impact on the strengthening of the subtropical zonal-mean zonal winds, which Simpson et al. (2016) found to be the main driver of the stationary wave response to climate change. This is also true across our model configurations (not shown). Following the reasoning of Simpson et al. (2016), this implies that any significant differences seen in the stationary wave response to climate change over the NH are predominantly due to the differences in the 1×CO2 basic state.

Figure 13a shows the v^* 300-hPa response to climate change in [0, 0]. It is quantitatively similar over North America to the CMIP5 mean shown in Simpson et al. (2016). The differences in the response between [B+, D] and [0, 0] are plotted in Fig. 13b. As with the response to increased drag in the 1×CO2 climatology, the impact of the additional parameterized orographic drag on the response to increased CO_2 scales with the amount of parameterized drag. This is demonstrated in Fig. 14, which shows the relationship between the RMS amplitude over the region indicated by the green box in Fig. 5 and, from left to right, the region over the Pacific (PC), the west coast of North America (WC), and the southwest interior of North America (SW), which are indicated by the green boxes in Fig. 13. There is a strong relationship between the climatological stationary wave amplitudes and their response to increased CO_2. There

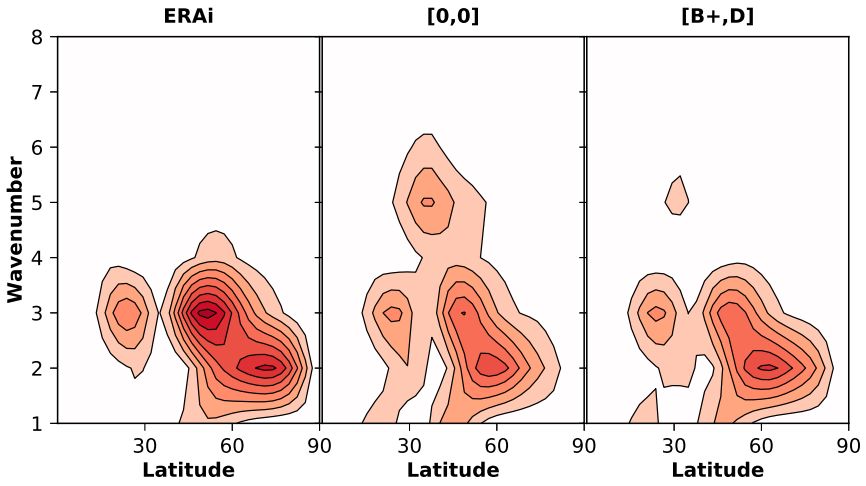

FIG. 11. DJF climatological v^* 300-hPa zonal wavenumber vs latitude spectrum for (left) ERA-Interim, (middle) [0, 0], and (right) [B+, D]. Contour interval is 5 $m^2 s^{-2}$.

is some spread around this relationship, however, and the position of the experiments along the linear fit vary somewhat, perhaps because of the discrete nature of the bounding box. These plots are illustrative and should be interpreted as such. In general, the experiments with the least amount of drag ([0, 0] and [B, 0]) have stronger historical stationary wave amplitudes over the Pacific and North America and exhibit stronger v^* responses. The experiments with the largest amount of drag ([B+, 0] and [B+, D]) have the weakest stationary waves over this region and have the weakest v^* responses.

Although the parameterized low-level drag acts to damp the stationary waves over the Pacific and North America, it acts to amplify them over the NA. One might then wonder whether the relationship described above holds for this region. Figure 15 shows the relationship between the RMS v^* amplitude over the region 30°–90°N, 45°W–45°E, versus the RMS amplitude of the response to increased CO_2 over the same sector. Once again the relationship is strong, with larger historical v^* amplitudes leading to a larger v^* response. However, as was shown in Fig. 10, the experiment [B+, 0] does not have a large increase in its v^* amplitude over the NA, despite having a large amount of parameterized drag. This is likely because of the difference between the Froude number dependences and centers of action of the blocking and the downslope wind component.

The dependence of the stationary wave response to climate change on the 1×CO2 basic state is anticipated from linear stationary wave theory. Following the

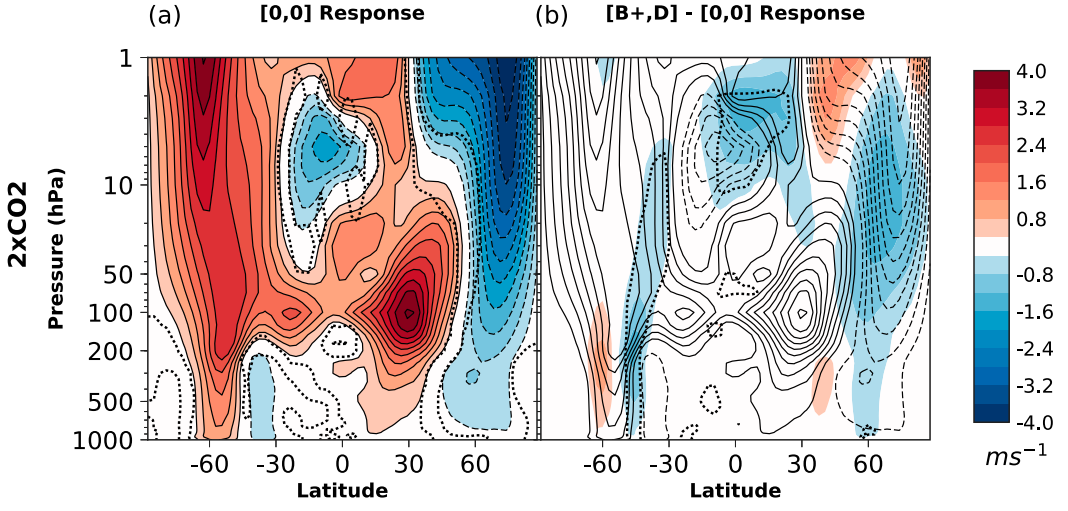

FIG. 12. DJF [u] response to climate change. (a) Response to climate change in [0, 0]; contour interval is 0.8 m s^{-1}. (b) Response to climate change in [B+, D] minus the response to climate change in [0, 0], with contour interval given by the color bar.

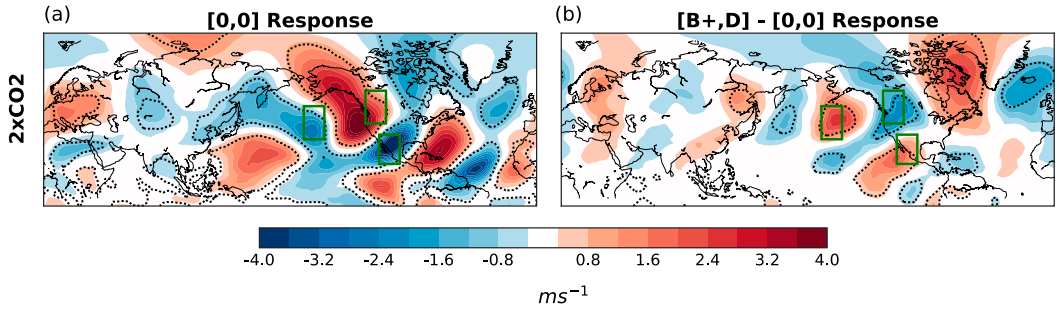

FIG. 13. DJF v^* 300-hPa response to climate change. (a) Response to climate change in [0, 0]. (b) Response to climate change in [B+, D] minus the response to climate change in [0, 0]. Contour interval given by the color bar.

derivations of Nigam and DeWeaver (2003) from the quasigeostrophic shallow-water equations, the amplitude of the stationary wave streamfunction for some arbitrary zonal k and meridional l wavenumber is given by

$$\hat{\psi} = \frac{f\hat{h}}{H[k^2 + l^2 - (\beta/[u])]}, \tag{7}$$

where $\beta = \partial f/\partial y$, H is the depth of the fluid, and $\hat{h}$ is the amplitude of the mechanical forcing by orography. Equation (7) shows that the amplitude of the stationary wave streamfunction depends linearly on the orographic forcing and, in a more complex way, on the zonal-mean zonal wind. By varying the orographic forcing through the orographic drag parameterization we find that there is a variation in the stationary wave response to climate change. Linear stationary wave theory suggests that this variation could be a result of either a different zonal-mean zonal wind response or the same zonal-mean zonal wind response acting on a different orographic forcing. Since Fig. 12 shows that the former is not significant between the experiments, it must be the latter, in which case the stationary wave response to climate change depends linearly on the orographic forcing.

b. Zonal wind response to climate change

The discussion presented in section 3c implies that the spread in the stationary wave response to climate change that results from varying the parameterized orographic drag may have an impact on the regional zonal wind response to climate change. Figure 16a shows the climatological MFC (solid black lines) and SEMFC (dashed black line) at 1×CO2 and their responses to climate change in red for experiments [0, 0] and [B+, D]. The orographic drag in the 2×CO2 climatology is also shown in gray. The first thing to note is that the orographic drag does not differ discernibly between the 1×CO2 and 2×CO2 climatologies (cf. with gray curve in Fig. 1), which implies that the influence of the orographic drag is limited to its impact on the 1×CO2 climatology and is not the direct cause of the differences in the response to CO_2 seen across the model configurations [see Sigmond and Scinocca (2010) for similar

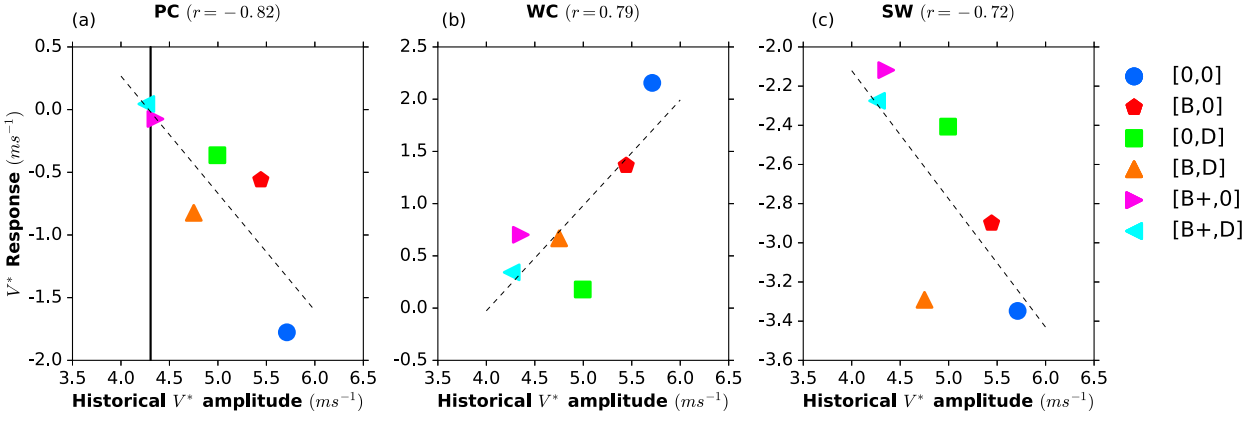

FIG. 14. Relationship between the DJF 1×CO2 climatological stationary wave amplitudes and their responses to climate change. The RMS v^* 300-hPa amplitude over 20°–45°N, 160°–60°W vs the v^* response over (a) PC, (b) WC, and (c) SW. PC, SW, and WC areas are indicated by green boxes in Fig. 13.The correlation coefficients r are indicated above the plots. Vertical line indicates ERA-Interim DJF climatological value.

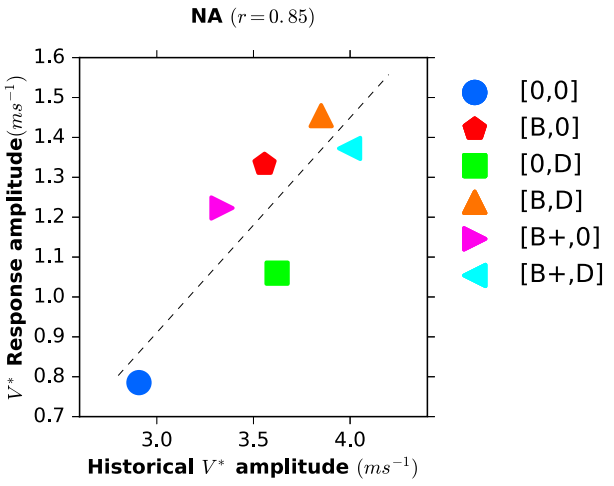

FIG. 15. Relationship between the DJF 1×CO2 climatological stationary wave amplitude over the NA and its response to climate change. RMS v^* 300-hPa amplitude calculated over 30°–90°N, 45°W–45°E. The correlation coefficient r is indicated above the plot.

arguments made in regards to gravity wave drag influences on the stratospheric polar vortex response to climate change]. The second is that the SEMFC (dashed red curves) dominates the response to climate change over the NH high latitudes, whereas the transient eddies dominate the response in the midlatitudes and over the SH. Figure 16b demonstrates how the 850-hPa zonal-mean zonal wind response to climate change follows the MFC response.

Figure 17 shows the longitudinal structure of the 850-hPa zonal wind response to climate change in [0, 0] and the difference in the response as a result of increased parameterized drag. Since climate change acts to weaken the climatological stationary waves over the NA (Fig. 13), one would expect an equatorward shift of the NA jet under climate change in these experiments, which is what is seen. There appears to be only a small subtle difference between the response in [0, 0] and [B+, D], but, on inspection of the zonal wind responses across the model configurations, particularly in [B, D], there is a pattern that emerges over the NA region. The experiments with larger amounts of low-level drag exhibit a larger strengthening of the winds over the Mediterranean region and a larger weakening of the winds over the Nordic seas, which equates to a larger equatorward shift of the NA jet.

Figure 18a shows the relationship between the historical jet latitude over the NA, indicated by the green sector over Europe in Fig. 17, and the jet latitude shift in response to climate change. There is a strong relationship between the two, with a more poleward-tilted jet having a larger equatorward shift under climate change. Although the internal variability is large over this region, as shown by the confidence intervals, subsetting of the data gives similar results, indicating that this

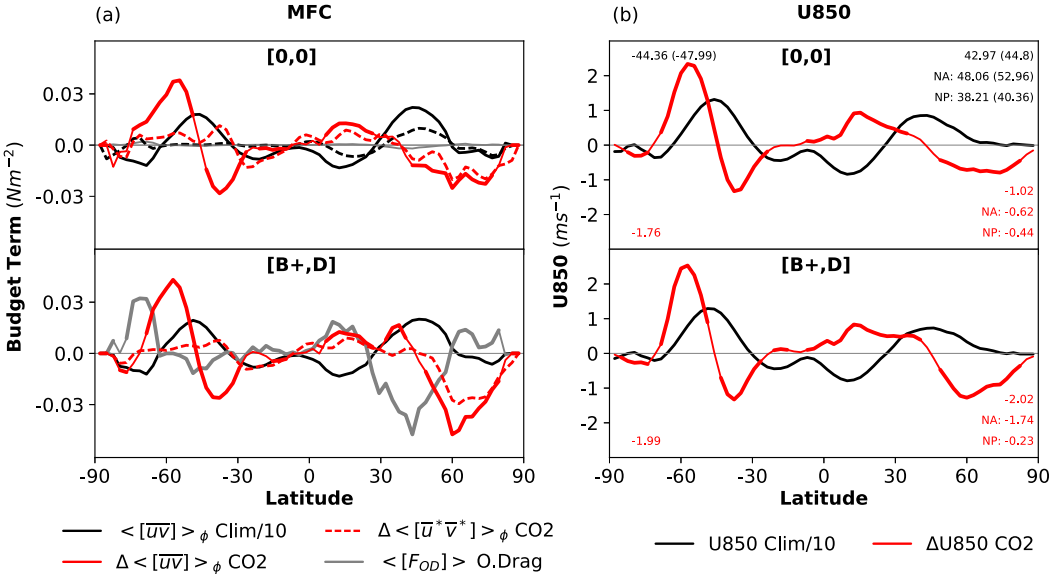

FIG. 16. (a) DJF 1×CO2 MFC climatology divided by 10 (solid black lines) and response to climate change (solid red lines). The dashed black line is the 1×CO2 climatological SEMFC in [0, 0] divided by 10. The solid gray line is the zonal-mean total (freely propagating, blocking, and downslope wind) parameterized orographic stress F_{OD} at 2×CO2. Dashed red lines are the SEMFC response to climate change. (b) DJF 1×CO2 u 850-hPa climatology divided by 10 (solid black lines) and response to climate change (solid red lines). Regions of statistically significant differences (at the 95% level based on the two-sided independent Student's t test) are indicated by a thickening of the line.

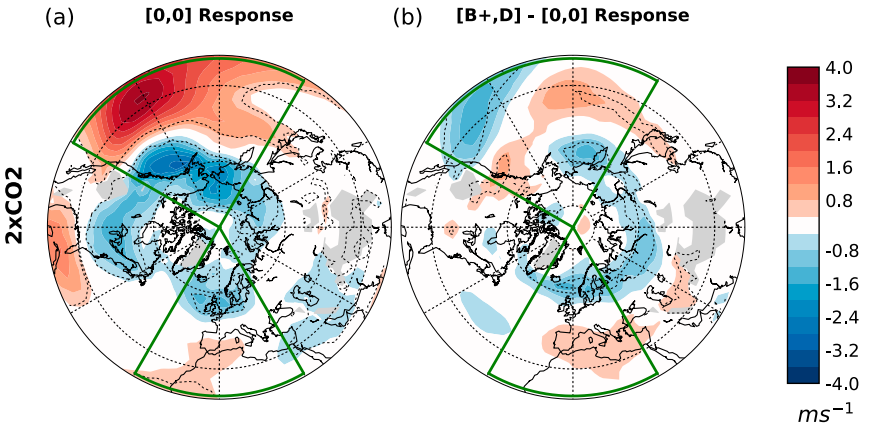

FIG. 17. DJF u 850-hPa response to climate change. (a) Response to climate change in [0, 0]. (b) Response to climate change in [B+, D] minus the response to climate change in [0, 0]. Contour interval given by the color bar.

relationship is robust. This is consistent with the relationship between the NA jet latitude and stationary wave amplitude presented in section 3.

The NP jet latitude response is generally very weak in these experiments (Fig. 18b). This is explained by the fact that the largest response to 2×CO2 is not in the node of the climatological winds but at the jet exit region over the North Pacific (see Fig. 3). This may also explain why there is no relationship between the climatology and the response (Fig. 18b). This does not mean that there cannot be a relationship under some other forcing in which the jet latitude shift over the NP is larger, however. While the jet latitude response to CO_2 is large over the SH, there is little relationship between the climatology and the response (Fig. 18), presumably because of the small role of stationary wave fluxes in the climate change response. The relationship between the climatological jet latitude and its response to climate change is also weak in the CMIP5 ensemble in DJF (Simpson and Polvani 2016, their Fig. 2d).

5. Discussion and conclusions

Through a set of experiments designed to systematically vary the magnitude of parameterized low-level orographic drag in CanAM4.1, we have shown that the stationary wave amplitudes and the zonal momentum transport by stationary waves in the NH wintertime are modulated by the strength of the low-level orographic drag. By looking first at the zonal wind response to increased parameterized drag in the 1×CO2 climatology, we found that there was a poleward shift of the midlatitude jets, the amplitude of which increases with increasing drag. Locally, the North Atlantic jet exhibited an increased poleward tilt away from western Europe, and there was a weakening of the winds over the central

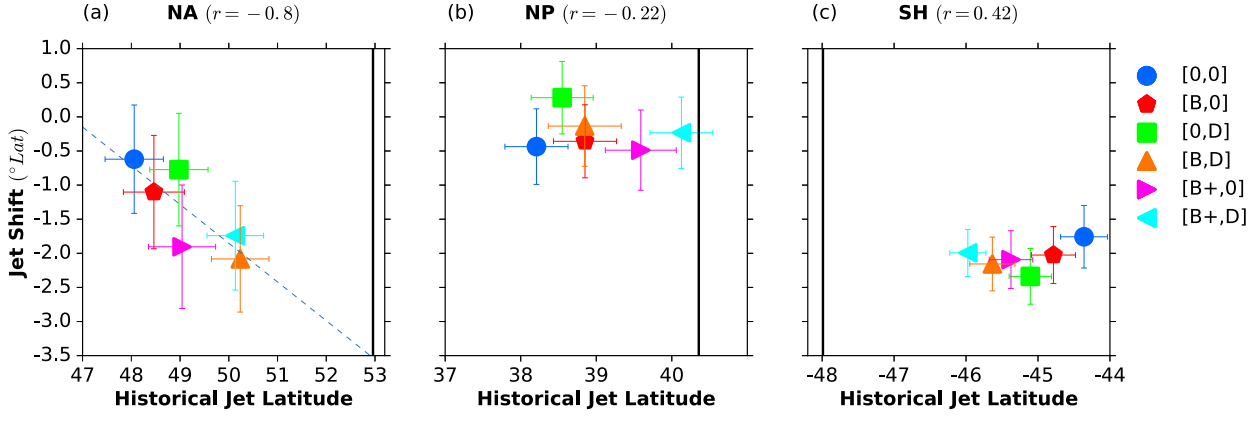

FIG. 18. Relationship between the DJF 1×CO2 climatological jet latitude and its response to climate change for (a) the NA, (b) the NP, and (c) the SH. The NA, NP, and SH region definitions are given in section 2c. The r values are indicated above the plots. Error bars correspond to the 95% confidence interval based on the two-sided independent Student's t test. Vertical line indicates ERA-Interim DJF climatological values.

Pacific and a strengthening of the winds over the North Pacific with increased drag. Together, these local changes lead to an improved representation of the zonal winds when compared with ERA-Interim.

We then identified that it is predominantly a change in the stationary eddy momentum flux convergence that contributes toward the change in the NH zonal winds with increased low-level orographic drag. Using the zonally asymmetric component of the meridional winds at 300 hPa to visualize the stationary wave field, we found that the increased drag leads to a damping of the waves over the North Pacific and an amplification of the waves over the North Atlantic. Spectral analysis of the meridional winds substantiates this and identifies that it is a damping of the zonal wavenumber-5 meridional winds over the midlatitudes and an amplification of wavenumber 2 over the high latitudes that lead to changes in the SEMFC. Focusing on the NA jet exit region, we show that there is a strong relationship between the stationary wave amplitudes over the Nordic seas and the NA jet latitude, with stronger stationary waves being associated with a more poleward NA jet. A comparison with the ERA-Interim meridional wind spectrum reveals not only that the wavenumber-5 amplitudes are too strong in midlatitudes and the wavenumber-2 amplitudes too weak at high latitudes in [0,0] but that these biases are also present in the CMIP5 multimodel-mean spectrum presented in Simpson et al. (2016).

It is important to acknowledge that not all models in the CMIP5 ensemble employ a low-level orographic drag scheme, and, if they do, the magnitude of this may vary greatly between them as a result of parameter uncertainty and tuning. Many are also of low horizontal resolution and have smoothed mean orography compared with reality. Since the low-level parameterized orographic drag has been shown to alter the stationary wave amplitudes over the middle and high latitudes, it is possible that the spread seen in the stationary wave amplitudes in the CMIP5 ensemble are a result of their representation of orography. Furthermore, since the SEMFC make the dominant contribution toward the MFC over the NH, it is likely that the equatorward jet biases and lack of NA jet tilt seen across the CMIP5 models are a reflection of biases in their stationary waves and associated momentum forcing. The biases in their stationary waves may be related to the treatment of subgrid orographic drag, since similar conclusions were drawn by Pithan et al. (2016) using a different model.

By prescribing SST and sea ice changes from coupled simulations in which the CO_2 was doubled, we demonstrated that the amplitude of the stationary wave response to climate change scales with the climatological stationary wave amplitudes over different regions. Over the Pacific and North America, where the increased orographic drag acts to reduce the stationary wave amplitudes, the meridional wind response to climate change was also reduced. On the other hand, over the NA, where increased orographic drag acted to amplify the stationary waves, the meridional wind response to climate change was increased with increasing orographic drag. These empirical results are consistent with linear stationary wave theory and suggest that the magnitude of the orographic forcing, which can be altered by the parameterized orographic drag, is important for the stationary wave response to climate change.

Many studies focus on the latitudinal shifting of the midlatitude jets under climate change, and, while we have shown that the stationary waves have an impact on the regional jet shift under climate change, they are also of interest in themselves. For example, in midlatitudes, large positive meridional wind anomalies lead to the advection of anomalously warm, moist air from the tropics which will have an impact on the local hydrology and temperatures (Nigam and DeWeaver 2003). Indeed, Simpson et al. (2016) demonstrated the close link between the meridional wind response over North America and the hydroclimate response there. The accurate projection of regional climate change therefore also depends on the accurate representation of the amplitude and location of stationary waves and their response to climate change.

The relationship between the historical stationary wave amplitudes and their response to climate change is likely to depend on the large-scale nature of the circulation response and thus on the SST and sea ice forcing we prescribed. Nonetheless, this study extends the body of work that highlights the importance of model fidelity and demonstrates that the spread in climatological basic states among models, as a result of parameter tuning or otherwise, can contribute to the uncertainty in the regional circulation response to climate change.

Acknowledgments. This study is supported by the ''Understanding the atmospheric circulation response to climate change'' (ACRCC, ERC Advanced Grant 339390) project. The first author would like to acknowledge the hospitality and support of CCCma during her visit there, when much of this work was completed. We thank Norm McFarlane for carefully reading the manuscript and providing helpful suggestions. The authors would also like to thank two anonymous reviewers for their contributions towards improving this manuscript.

REFERENCES

Barnes, E. A., and D. L. Hartmann, 2010: Testing a theory for the effect of latitude on the persistence of eddy-driven jets using CMIP3 simulations. *Geophys. Res. Lett.*, **37**, L15801, doi:10.1029/2010GL044144.

——, and L. Polvani, 2013: Response of the midlatitude jets, and of their variability, to increased greenhouse gases in the CMIP5 models. *J. Climate*, **26**, 7117–7135, doi:10.1175/JCLI-D-12-00536.1.

Bracegirdle, T. J., E. Shuckburgh, J. B. Sallee, Z. Wang, A. J. S. Meijers, N. Bruneau, T. Phillips, and L. J. Wilcox, 2013: Assessment of surface winds over the Atlantic, Indian, and Pacific Ocean sectors of the Southern Ocean in CMIP5 models: Historical bias, forcing response, and state dependence. *J. Geophys. Res. Atmos.*, **118**, 547–562, doi:10.1002/jgrd.50153.

Brayshaw, D. J., B. J. Hoskins, and M. Blackburn, 2009: The basic ingredients of the North Atlantic storm track. Part I: Land–sea contrast and orography. *J. Atmos. Sci.*, **66**, 2539–2558, doi:10.1175/2009JAS3078.1.

Butler, A. H., D. W. J. Thompson, and R. Heikes, 2010: The steady-state atmospheric circulation response to climate change–like thermal forcings in a simple general circulation model. *J. Climate*, **23**, 3474–3496, doi:10.1175/2010JCLI3228.1.

Charney, J. G., and A. Eliassen, 1949: A numerical method for predicting the perturbations of the middle latitude westerlies. *Tellus*, **1**, 38–54, doi:10.3402/tellusa.v1i2.8500.

Chen, G., and P. Zurita-Gotor, 2008: The tropospheric jet response to prescribed zonal forcing in an idealized atmospheric model. *J. Atmos. Sci.*, **65**, 2254–2271, doi:10.1175/2007JAS2589.1.

Dee, D. P., and Coauthors, 2011: The ERA-Interim reanalysis: Configuration and performance of the data assimilation system. *Quart. J. Roy. Meteor. Soc.*, **137**, 553–597, doi:10.1002/qj.828.

Delsole, T., and J. Shukla, 2010: Model fidelity versus skill in seasonal forecasting. *J. Climate*, **23**, 4794–4806, doi:10.1175/2010JCLI3164.1.

DeWeaver, E., and S. Nigam, 2000: Do stationary waves drive the zonal-mean jet anomalies of the northern winter? *J. Climate*, **13**, 2160–2176, doi:10.1175/1520-0442(2000)013<2160:DSWDTZ>2.0.CO;2.

Golledge, N. R., D. E. Kowalewski, T. R. Naish, R. H. Levy, C. J. Fogwill, and E. G. W. Gasson, 2015: The multi-millennial Antarctic commitment to future sea-level rise. *Nature*, **526**, 421–425, doi:10.1038/nature15706.

Grose, W. L., and B. J. Hoskins, 1979: On the influence of orography on large-scale atmospheric flow. *J. Atmos. Sci.*, **36**, 223–234, doi:10.1175/1520-0469(1979)036<0223:OTIOOO>2.0.CO;2.

Junge, M. M., R. Blender, K. Fraedrich, V. Gayler, U. Luksch, and F. Lunkeit, 2005: A world without Greenland: Impacts on the Northern Hemisphere winter circulation in low- and high-resolution models. *Climate Dyn.*, **24**, 297–307, doi:10.1007/s00382-004-0501-2.

Kharin, V. V., and J. F. Scinocca, 2012: The impact of model fidelity on seasonal predictive skill. *Geophys. Res. Lett.*, **39**, L18803, doi:10.1029/2012GL052815.

Kidston, J., and E. P. Gerber, 2010: Intermodel variability of the poleward shift of the austral jet stream in the CMIP3 integrations linked to biases in 20th century climatology. *Geophys. Res. Lett.*, **37**, L09708, doi:10.1029/2010GL042873.

Laprise, R., and C. Girard, 1990: A spectral general circulation model using a piecewise-constant finite-element representation on a hybrid vertical coordinate system. *J. Climate*, **3**, 32–52, doi:10.1175/1520-0442(1990)003<0032:ASGCMU>2.0.CO;2.

Limpasuvan, V., and D. L. Hartmann, 2000: Wave-maintained annular modes of climate variability. *J. Climate*, **13**, 4414–4429, doi:10.1175/1520-0442(2000)013<4414:WMAMOC>2.0.CO;2.

Lott, F., and M. J. Miller, 1997: A new subgrid-scale orographic drag parametrization: Its formulation and testing. *Quart. J. Roy. Meteor. Soc.*, **123**, 101–127, doi:10.1002/qj.49712353704.

Manzini, E., and Coauthors, 2014: Northern winter climate change: Assessment of uncertainty in CMIP5 projections related to stratosphere–troposphere coupling. *J. Geophys. Res. Atmos.*, **119**, 7979–7998, doi:10.1002/2013JD021403.

McFarlane, N. A., 1987: The effect of orographically excited gravity wave drag on the general circulation of the lower stratosphere and troposphere. *J. Atmos. Sci.*, **44**, 1775–1800, doi:10.1175/1520-0469(1987)044⟨1775:TEOOEG⟩2.0.CO;2.

McLandress, C., T. G. Shepherd, S. Polavarapu, and S. R. Beagley, 2012: Is missing orographic gravity wave drag near 60°S the cause of the stratospheric zonal wind biases in chemistry climate models? *J. Atmos. Sci.*, **69**, 802–818, doi:10.1175/JAS-D-11-0159.1.

Nigam, S., and E. DeWeaver, 2003: Stationary waves (orographic and thermally forced). *Encyclopedia of Atmospheric Sciences*, 1st ed. Academic Press, 2121–2137.

Palmer, T. N., G. J. Shutts, and R. Swinbank, 1986: Alleviation of a systematic westerly bias in general circulation and numerical weather prediction models through an orographic gravity wave drag parametrization. *Quart. J. Roy. Meteor. Soc.*, **112**, 1001–1039, doi:10.1002/qj.49711247406.

Pithan, F., T. G. Shepherd, G. Zappa, and I. Sandu, 2016: Climate model biases in jet streams, blocking and storm tracks resulting from missing orographic drag. *Geophys. Res. Lett.*, **43**, 7231–7240, doi:10.1002/2016GL069551.

Plumb, R. A., 1985: On the three-dimensional propagation of stationary waves. *J. Atmos. Sci.*, **42**, 217–229, doi:10.1175/1520-0469(1985)042<0217:OTTDPO>2.0.CO;2.

Rossby, C.-G., 1939: Relation between variations in the intensity of the zonal circulation of the atmosphere and the displacements of the semi-permanent centers of action. *J. Mar. Res.*, **2**, 38–55, doi:10.1357/002224039806649023.

Sandu, I., P. Bechtold, A. Beljaars, A. Bozzo, F. Pithan, T. G. Shepherd, and A. Zadra, 2016: Impacts of parameterized orographic drag on the Northern Hemisphere winter circulation. *J. Adv. Model. Earth Syst.*, **8**, 196–211, doi:10.1002/2015MS000564.

Scinocca, J. F., and N. A. McFarlane, 2000: The parametrization of drag induced by stratified flow over anisotropic orography. *Quart. J. Roy. Meteor. Soc.*, **126**, 2353–2393, doi:10.1002/qj.49712656802.

——, ——, M. Lazare, J. Li, and D. Plummer, 2008: The CCCma third generation AGCM and its extension into the middle atmosphere. *Atmos. Chem. Phys.*, **8**, 7055–7074, doi:10.5194/acp-8-7055-2008.

Shepherd, T. G., 2014: Atmospheric circulation as a source of uncertainty in climate change projections. *Nat. Geosci.*, **7**, 703–708, doi:10.1038/ngeo2253.

Sigmond, M., and J. F. Scinocca, 2010: The influence of the basic state on the Northern Hemisphere circulation response to climate change. *J. Climate*, **23**, 1434–1446, doi:10.1175/2009JCLI3167.1.

Simpson, I. R., and L. M. Polvani, 2016: Revisiting the relationship between jet position, forced response, and annular mode variability in the southern midlatitudes. *Geophys. Res. Lett.*, **43**, 2896–2903, doi:10.1002/2016GL067989.

——, T. A. Shaw, and R. Seager, 2014: A diagnosis of the seasonally and longitudinally varying mid-latitude circulation response to global warming. *J. Atmos. Sci.*, **71**, 2489–2515, doi:10.1175/JAS-D-13-0325.1.

——, R. Seager, M. Ting, and T. A. Shaw, 2016: Causes of change in Northern Hemisphere winter meridional winds and regional hydroclimate. *Nat. Climate Change*, **6**, 65–70, doi:10.1038/nclimate2783.

Tibaldi, S., 1986: Envelope orography and maintenance of the quasi-stationary circulation in the ECMWF global models. Advances in Geophysics, Vol. 29, Academic Press, 339–374, doi:10.1016/S0065-2687(08)60045-X.

Ting, M., M. P. Hoerling, T. Xu, and A. Kumar, 1996: Northern Hemisphere teleconnection patterns during extreme phases of the zonal-mean circulation. *J. Climate*, **9**, 2614–2633, doi:10.1175/1520-0442(1996)009<2614:NHTPDE>2.0.CO;2.

van Niekerk, A., T. G. Shepherd, S. B. Vosper, and S. Webster, 2016: Sensitivity of resolved and parametrized surface drag to changes in resolution and parametrization. *Quart. J. Roy. Meteor. Soc.*, **142**, 2300–2313, doi:10.1002/qj.2821.

von Salzen, K., and Coauthors, 2013: The Canadian Fourth Generation Atmospheric Global Climate Model (CanAM4). Part I: Representation of physical processes. *Atmos.–Ocean*, **51**, 104–125, doi:10.1080/07055900.2012.755610.

Vosper, S. B., 2000: Three-dimensional numerical simulations of strongly stratified flow past conical orography. *J. Atmos. Sci.*, **57**, 3716–3739, doi:10.1175/1520-0469(2000)057<3716:TDNSOS>2.0.CO;2.

Wallace, J. M., and H. Hsu, 1985: Another look at the index cycle. *Tellus*, **37A**, 478–486, doi:10.1111/j.1600-0870.1985.tb00445.x.

Woollings, T., A. Hannachi, and B. Hoskins, 2010: Variability of the North Atlantic eddy-driven jet stream. *Quart. J. Roy. Meteor. Soc.*, **136**, 856–868, doi:10.1002/qj.625.

Zadra, A., and Coauthors, 2013: WGNE Drag Project. Accessed 26 June 2017. [Available online at http://collaboration.cmc.ec.gc.ca/science/rpn/drag_project/.]

Zappa, G., and T. G. Shepherd, 2017: Storylines of atmospheric circulation change for European regional climate impact assessment. *J. Climate*, in press.

——, L. C. Shaffrey, K. I. Hodges, P. G. Sansom, and D. B. Stephenson, 2013: A multimodel assessment of future projections of North Atlantic and European extratropical cyclones in the CMIP5 climate models. *J. Climate*, **26**, 5846–5862, doi:10.1175/JCLI-D-12-00573.1.